International Journal of Heat and Mass Transfer 52 (2009) 1534–1539

Contents lists available at ScienceDirect

International Journal of Heat and Mass Transfer

journal homepage: www.elsevier.com/locate/ijhmt

Bubble generation in micro-volumes of "nanofluids"

L. Vasiliev *, E. Hleb, A. Shnip, D. Lapotko

A.V. Lykov Heat and Mass Transfer Institute, 15 P. Brovka Street, Minsk 220072, Belarus

ARTICLE INFO

Article history:
Received 15 August 2008
Available online 8 October 2008

Keywords:
Bubbles
Nanoparticles
Vaporization
Photothermal

ABSTRACT

We report experimental investigation of a transparent flat mini evaporator heated by laser beam. The influence of non-absorbing and absorbing nanoparticles immersed in pure water, and heat absorbing fluid on the heat transfer intensification was analyzed. Nanoparticles may initiate vaporization and boiling of fluid at low heat input. Providing specific task and conditions the nanoparticles may be used in passive or active modes. Passive mode assumes that nanoparticles do not generate thermal energy and improve bubble nucleation conditions due to additional nucleation of the fluid, thus decreasing boiling/vaporization temperature thresholds. Active mode assumes that nanoparticles act as converters of optical energy into thermal one.

1. Introduction

Nucleation of the boiling of liquids is the subject of numerous studies, which cover questions related to formation of bubble nuclei in metastable liquids. Particle deposition as bubble generator on extended surfaces of heat transfer was studied earlier [1–3]. The general conclusion is that micro and nano particles on the heat loaded surface initiate a bubble generation and enhance two-phase heat transfer. Micro heat pipe effect inside the porous structure with two-phase forced convection in the annular minichannel could be considered thermodynamically as an efficient mini-evaporator and effective cooling device for micro and optoelectronic components [4]. Actually a new class of heat transfer fluids was developed that are referred as "Nanofluids". Nanofluids are engineered by suspending ultra-fine metallic or nonmetallic nanometer particles in traditional fluids such as water, oil, hydrocarbons. Some experimental investigations have revealed that nanofluids have remarkably higher thermal conductivity and greater heat transfer characteristics than conventional pure fluids [5–15]. All above mentioned experiments with nanofluids in heat pipes were performed with conventional heat pipe envelopes made from metal.

In some cases it is interesting to perform heat pipe envelope from transparent material (glass, plastic) and to deliver the heat to the pipe evaporator by radiation. Bubble generation in mini volumes is responsible for nanofluid circulation in the loop. The bubbles are considered as a motion force to organize the fluid circulation in pulsating heat pipes and thermosyphons, Fig. 1. Such type of two-phase cooling system, for example, have a good perspective for space applications. Transparent evaporators made from glass or plastic have also a real practical potential for mini/micro fuel cells thermal control, photoelectronic components cooling. Transparent condensers are interesting to be cooled by radiation in the space. High temperature heat transfer devices can be used in power stations as transparent (glass) pulsating heat pipes in the air preheaters for furnaces and boilers.

One of the major goals of this paper is the experimental investigation of the influence of metal NPs immersed in water media on the bubble generation and two-phase heat transfer intensification. We have previously shown [16,17] that the heat flow generated by light-absorbing nanoparticles (NP) such as gold NPs initiates bubble generation when short laser pulses are used as primary sources of thermal energy. Under these conditions the temporal scale of photothermal conversion of the energy is limited by duration of laser pulse and provides good thermal confinement of the heat released in NPs through excitation of plasmon modes in those particles. The main role of such NPs was to generate the heat. The limitation of this method for vaporization is in delivery of the energy into the point of interest: it should be optically transparent to allow the radiation to reach for the NPs. Our previous studies of bubble generation around NPs has stimulated the hypothesis that regardless the source of thermal energy the presence of NPs of certain size in heated media may influence the process of bubble nucleation and development [3].

The other goal is related to the role of non-absorbing NP as the initiator of bubble in the light-absorbing working fluid, for example, homogenous solution of light-absorbing dye –Trypan Blue (T8154, Sigma–Aldrich Corp., St. Louis, MO). NPs are considered now as additional centres of nucleation due to increased surface of liquid/solid interaction. Are NPs in such a case stimulates the

* Corresponding author. Tel./fax: +375 172 84 21 33.
E-mail address: Leonard_Vasiliev@rambler.ru (L. Vasiliev).

0017-9310/$ - see front matter © 2008 Elsevier Ltd. All rights reserved.
doi:10.1016/j.ijheatmasstransfer.2008.08.009

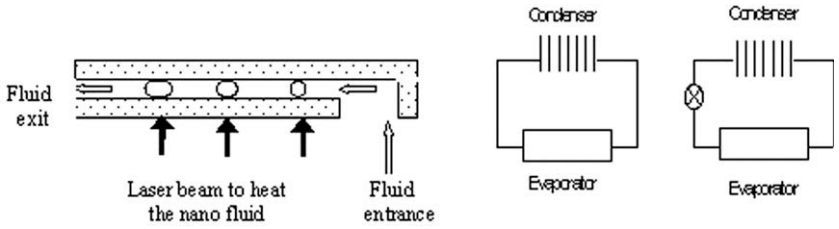

Fig. 1. Schematic of the mini evaporator with transparent walls heated by pulsed laser beam.

appearance of earlier threshold of vapour generation? The aim of current experimental work was to validate this hypothesis and evaluate the influence of "passive" NPs, as the element of heterogeneity in the fluid on the decrease of the energy threshold of bubble generation.

2. Method and materials

2.1. Photo-induced thermal phenomena

After absorption of a laser pulse the non-radiative relaxation of optical energy occurs within 10^{-11} s [18]. This is approximately the time of initial heating of absorbing areas that act as heat sources as long as a laser pulse lasts. The next process is the heat diffusion into surrounding media with a characteristic time τ_d that depends mainly upon the size r_a of a spherically symmetrical light-absorbing area:

$$\tau_d = 0.9011 \frac{r_a^2}{a}, \tag{1}$$

where a – the heat diffusion coefficient, τ_d is defined as time of temperature decrease by 10 times.

Comparing laser pulse duration τ_{pump} to cooling time τ_d we consider two modes: a short pulse mode ($\tau_{pump} \ll \tau_d$) when all thermal energy is immediately released within the absorbing area, and a quasi-stationary mode (long-pulse mode) when the laser pulse width is much longer than cooling time τ_d ($\tau_{pump} \gg \tau_d$).

These two modes have different dynamics of the photo-induced thermal field. Depending on the initially induced temperature we will also consider the linear mode of laser-medium interaction when only heating and cooling processes occur (temperature is proportional to deposited laser energy) and the non-linear mode which assumes phase transitions when temperatures exceed the vaporization threshold (temperature is no longer proportional to deposited energy).

For samples with uniform absorption of laser pulse and excluded any potential local absorbers initial temperatures induced in a sample after absorption of short laser pulse (all energy is released within absorbing volume) were calculated as:

$$\Delta T = \alpha(\lambda) \frac{\varepsilon}{\rho C}, \tag{2}$$

where α is the light absorption coefficient of media at the light wavelength λ, ρ is the density, ε is the laser pulse fluence, and C is the heat capacity.

The photo-induced bubbles may emerge when the photo-induced temperature reaches the critical value (this mechanism is referred to as local overheating). Also the bubbles may be induced by rarefaction waves. We assume that light intensities are below the optical breakdown threshold, thus the two mechanisms are assumed. The probability of bubble generation and its dynamics greatly depend upon the properties of initial heterogeneity around which a bubble emerges. We will analyze the dynamics of a bubble radius $R(t)$. The basic equation that describes the bubble behavior at the stage when pressure stress has already relaxed (i.e., at stages after first nanoseconds) is the Rayleigh–Plesset equation [19–21]:

$$R\frac{d^2R}{dt^2} + \frac{3}{2}\left(\frac{dR}{dt}\right)^2 = \frac{1}{\rho}\left(P_v(t) - P_\infty - \frac{2\sigma}{R} - \frac{4\eta}{R}\frac{dR}{dt}\right), \tag{3}$$

where σ is the surface tension coefficient, η is the viscosity, P_∞ is the outer pressure, and P_v is the inner pressure.

For short laser pulses the most universal mechanism of bubble formation is vaporization of liquid with the initial vapor pressure being equal to critical pressure P_{v_0}[22]. For initial conditions such as:

$$\frac{dR}{dt} = 0, R = R_0 \text{ at } t = o \tag{4}$$

Eq. (3) was solved numerically to obtain $R(t)$ under assumption of adiabatic approximation of bubble expansion:

$$P_v(t) = P_{v0} \cdot \left(\frac{R_0^3}{R(t)^3}\right)^\gamma, \tag{5}$$

where γ is the adiabatic coefficient, and P_{vo} is initial pressure in the bubble.

In the non-linear mode we use two basic input parameters: R_0 as the radius of heterogeneity that gives birth to the bubble and P_{v0} as initial pressure that depends upon absorbed optical energy. The output parameters that can be obtained numerically are bubble duration (lifetime) and maximal radius. As well as temperatures they cannot be measured directly and are analyzed below with the thermal lens approach through the parameters of a probe laser beam.

2.2. Experimental set up

Fluid was heated through absorption of short laser pulse (532 nm, 10 ns duration at the level 0.5 of maximum, 16.5 μm diameter at the level 0.5 of maximum) (LS-2132 laser, Lotis TII, Minsk, Belarus). Such pulse parameters provided heat-confined condition when all absorbed energy is released within the absorbing volume before heat diffusion takes place.

Photothermal generation and detection of vapor bubbles in liquid was performed using the photothermal (PT) microscope previously developed by us [23]. Photo-induced bubbles were detected and measured by the optical method – thermal lens. Probe beam detection is realized through the thermal lens scheme (Fig. 2): the probe laser beam (He–Ne laser, model LGN-224, Russia, 633 nm, 0.2 mW, beam diameter at sample plane 22 μm) passes through the object, the collecting lens, then through the axial pinhole and is registered with photodetector. The output signal from the photodetector was registered with a digital oscilloscope (computer board Bordo-211 from Diagnostic Systems, Belarus) with 10 ns temporal resolution and analyzed by a computer. In absence of the bubbles the amplitude of thermal lens signal is roughly proportional to an averaged temperature in the probed volume. While absolute measurement of the temperature requires

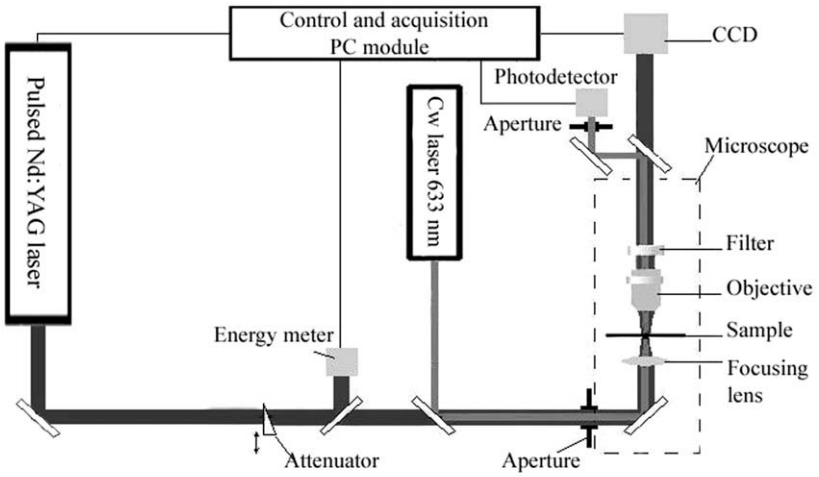

Fig. 2. Optical scheme of photothermal set up for pulsed heating of the micro-volume and optical imaging and measuring laser-induced bubbles.

sophisticated calibration procedure we may use PT signal amplitude for relative measurements of the changes of the temperature relatively to its initial level prior to application of laser radiation. Pulse fluence is obtained through measuring pulse energy with energy meter that was calibrated with Ophir energy meter (PE10-SH, Ophir Optonics, Ltd., Israel) and through measuring the diameter of laser spot in the sample plane with CCD image detector (Luca DL-658 M-TIL, Andor Technology, Ireland). In parallel the vapor bubbles were imaged with time-gated CCD camera and using the portion of pump laser pulse to form the image.

Heating–cooling process and the bubble arrival produce different PT-responses of specific shapes and in the case of bubble the duration of PT-response indicates bubble lifetime and size [16,24]. In each sample 50–100 PT-responses to laser pulse were obtained so each response represented one point of solution that was irradiated with only one pulse at specified energy (fluence). Then the probability of bubble occurrence was calculated as:

$$\mathrm{PRB} = \frac{N}{M}, \tag{6}$$

where M – amount of irradiated objects, N – amount of bubble-specific responses.

The values of PRB were obtained at several laser pulse fluencies so that the one corresponding to PRB being 0.5 was defined as bubble generation threshold $\varepsilon(0.5)$ for a given sample.

2.3. Samples

Three types of samples were studies.

(1) *Homogenous solution of light-absorbing dye –Trypan Blue* (T8154, Sigma–Aldrich Corp., St. Louis, MO). The solution was studied as a sealed volume between two parallel glasses – slide and cover glass. For a gap between the glasses – 120 μm – we have used gaskets between the glasses (S-24737, Molecular Probes Inc., Eugene, OR). Such preparation provided uniform absorption of laser pulse in the sample volume and excluded any potential local absorbers. In this case heated space was confined by laser beam diameter and vertical gap between the glasses.

(2) *Suspension of Al_2O_3 nanoparticles in a solution of Trypan Blue*. Suspension of non-absorbing nanoparticles were prepared by diluting Al_2O_3 nanoparticles by distilled water. For preparing suspension of nanoparticles with diameter <220 nm initial suspension was filtered through 0.22 μm micro-pore filter (#SLGS0250S, Millipore Corporation, Bedford, MA) and then it was added into Trypan Blue solution. This solution was studied in the same geometry as for homogeneous solution of Trypan Blue (Fig. 3 (left)).

(3) Water suspension of light-absorption gold nanoparticles: we have studied 3 types of gold NPs (spheres, rods, shells). Spheres with 30 nm diameter were obtained from Ted Pella Inc. (#15706, Redding, CA). Spheres have one plasmon resonance at 520 nm. Gold rods (NR) with the diameter 14 nm and the length of 45 nm were prepared as described in [25]. We have used high-yield suspension of gold rods with very low content of spherical particles. The rods have transverse plasmon resonance at 530 nm and the main longitudinal plasmon resonance at 750 nm. The shells (NS) consisting of the silica core and gold shell with the outer diameter of 170 nm were prepared as described in [26]. All NPs were prepared as water suspension at the concentration of $2.5^{*}10^{11}$/ml that provided average inter-particle distance of 1.7 μm. For PT microscopy we have prepared the samples in the same geometry as for homogeneous solution of Trypan Blue.

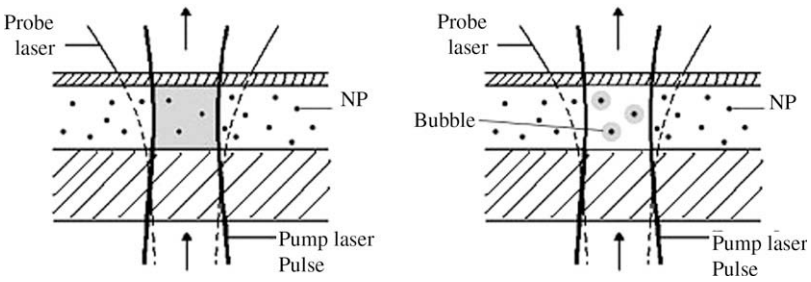

Fig. 3. Experimental model: (left) laser-induced heating of the volume with non-absorbing nanoparticles, (right) generation of laser-induced bubbles around gold light-absorbing nanoparticles; single pump laser pulse: 532 nm, 10 ns.

The light absorption coefficients of all samples were measured with spectrophotometer (USB 650 Red Tide, Ocean Optics, Inc, Dunedin, FL) in standard 1.5 ml cuevettes with 1 cm optical path.

3. Results and discussion

3.1. Optical detection and characterization of vaporization process in micro-volume

In all studied samples the bubble–specific photo-thermal signals (Fig. 4) – PT-responses and PT-images – were detected. Bubble-specific PT –response has negative symmetrical profile which front describes bubble expansion and the tail describes bubble collapse. Length of bubble-related signal response indicates bubble lifetime (Fig. 4 (left)). In homogeneous media bubbles emerged in all area of the pump laser beam. The diameter of the bubbles is much smaller than that for heated volume (cell or laser beam) (Fig. 4 (right)). Regardless of the medium the bubble generation process had statistical nature with bubble generation probability PRB from 0 to 1.

3.2. Vaporization and non-absorbing (passive) nanoparticles

We have discovered that presence of passive (non-absorbing) NPs in light-absorbing fluid increases probability of bubble generation (Fig. 5). At laser fluence 1.2 J/cm^2 the bubble generation probability increased from 0.32 for pure fluid to 0.64 for the same fluid with non-absorbing NPs, the boiling point was decreased from 1.8 J/cm^2 for pure fluid to 1.0 J/cm^2 for the fluid with NPs. Also we observed an increase of bubble lifetime after adding NPs into heated fluid (Fig. 6b).

The presence of passive (non-absorbing) NPs in the heated liquid has caused the decrease of bubble generation energy and temperature thresholds (Fig. 6a). This effect was found to be temperature-dependent and at optimal concentration of the NPs may allow to decrease thermal power threshold almost by half relatively to that for homogenous liquid without any NPs. At the same time the concentration of the NPs does not influence average lifetime (and hence the maximal diameter) of the bubbles (Fig. 6b) that are generated in the heated liquid.

However more detailed analyses of statistical distribution of the bubble lifetimes has revealed that adding the NPs into the liquid does influence the bubble lifetime and hence the bubble maximal diameter (Fig. 7). First, NPs have caused generation of the bubbles with the lifetime being almost twice longer than the lifetime of the

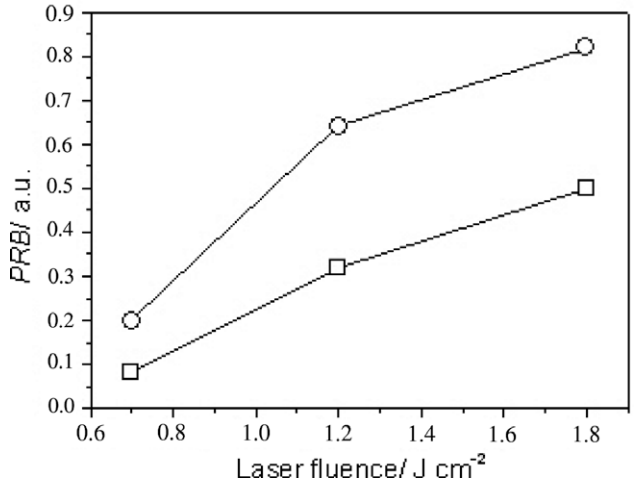

Fig. 5. Dependence of bubble generation probability in transparent micro-evaporator upon laser influence: □, pure homogeneous fluid, ○, the same fluid with non-absorbing nanoparticles.

bubbles being generated in the homogenous liquid and without the NPs. In the samples with NPs we have discovered the two sub-populations of the bubbles. First subpopulation has the histogram being similar to that of control (liquid without NPs) and the second sub-population consists of significantly bigger bubbles having the lifetime depending upon the size of NPs. For a relatively small NPs the lifetime of the bubbles in this specific sub-population has increased by 2–3 times (Fig. 7). For larger NPs with the dimensions in the range between 220 and 1000 nm the lifetime of the bubbles was found to be 4–8 times longer than that for control. Further increase of the NP dimensions (above 1000 nm) has caused the histogram being very close to that of control. This may indicate that the effect of the stimulation of bubble generation is size-dependent and is most pronounced with nanoparticles but almost disappears when the size of the particles increases up to micrometer range.

Potential explanations of this effect may include such factors as:

NPs are the fluctuations of the density that act as sites for bubble nucleation under lower temperatures. An invariant character of bubble lifetime means that the potential energy of the bubble does not depend upon the presence of NPs and this is quite natural because this energy depends upon the source of initial energy and in this case it is a liquid, not the NPs. Therefore the potential role of

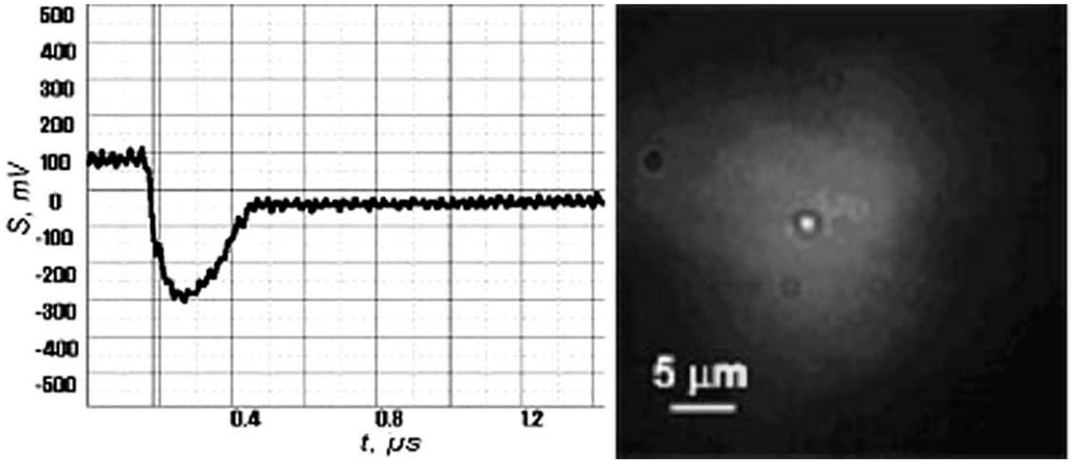

Fig. 4. Photo-thermal signals obtained from individual bubbles generated in transparent micro-evaporator: PT-response with bubble-specific shape (left) and PT-image (right). Y-axis is for the output of the photodetector (mV).

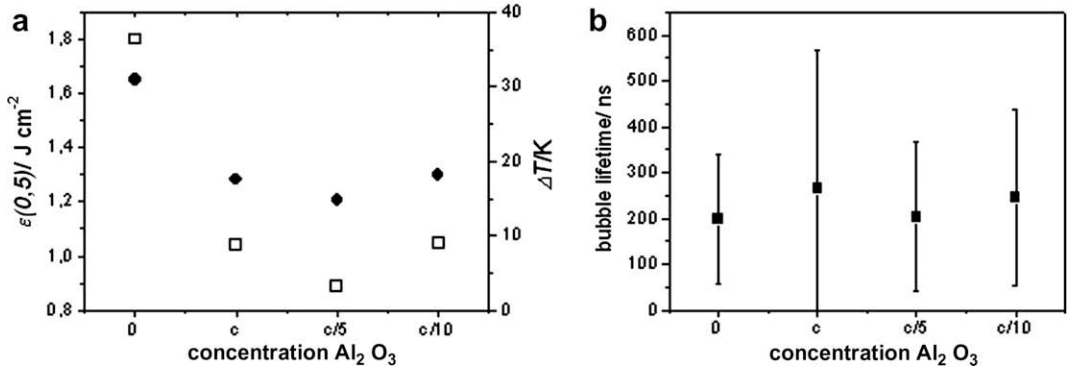

Fig. 6. (A): Bubble generation threshold (□)/laser-induced temperature (♦) and (B) average bubble lifetime at laser fluence 0.7 J/cm^2 upon the concentration of Al_2O_3 nanoparticles.

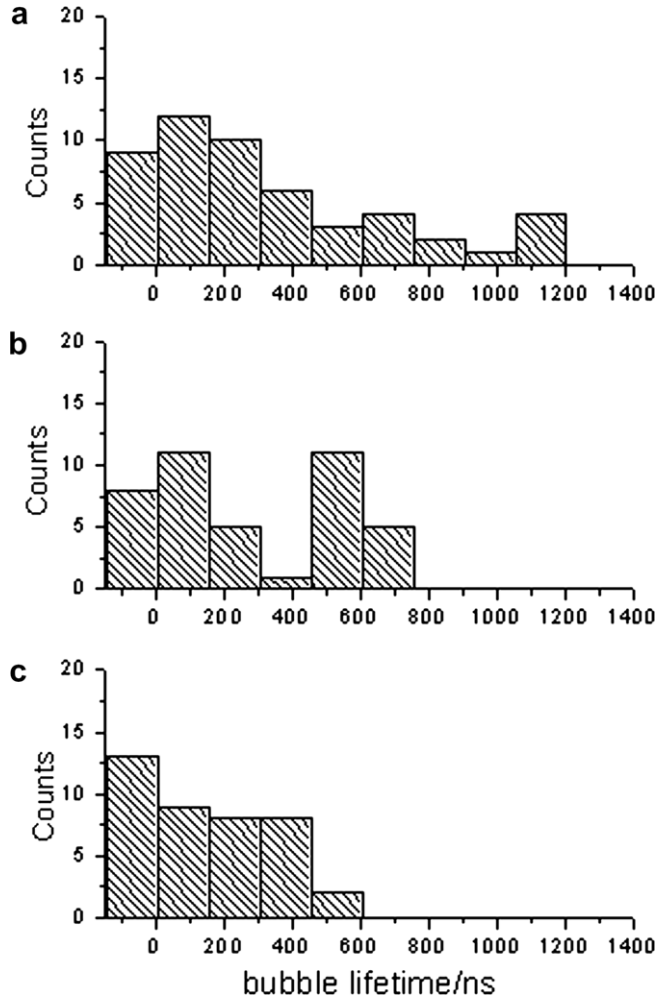

Fig. 7. Histograms of the bubble lifetime for homogenous solution (a), at laser fluence 2.34 J/cm^2 (b), 200–1000 nm (c), for the suspensions of Al_2O_3 nanoparticles with the size 0–200 nm.

the NPs may be associated with modification of bubble nucleation process.

3.3. Vaporization and light-absorbing (active) nanoparticles

This model had the same optical absorption coefficient for the bulk volume as the previous one. The difference from the previous model was in using absorbing NPs and non-absorbing liquid (water). Application of the same laser pulse (0.7 J/cm^2) has caused much bigger bubbles in suspension of gold nanoshells with the duration being 2 times longer comparing with the case of homogeneous optical absorbance. We have measured the dependence of the bubble generation probability upon laser fluence and so have determined bubble generation energy threshold: 8 J/cm^2 for gold nanorods, 1.8 J/cm^2 for gold spheres 30 nm and 70 mJ/cm^2 for gold nanoshells. Latest is 25 times lower than the threshold obtained for homogeneous model and 14 times lower comparing to the threshold of the model with "passive" NPs. In this case we could not use the expressions Eq. (2) for calculating initial laser-induced temperature of the gold NP because the dynamics of its heating should take into consideration the heat transfer between the NP and surrounding liquid and also the process of vaporization that may develop much faster than the laser pulse (according to the nucleation time may be about 100 ps while the pulse duration is 100 times longer −10 ns).

However we have analyzed experimentally by using PT-response the relative change of the bulk temperature during generation of the bubbles. We have observed the bubbles at the fluence of pump laser pulse being 11 J/cm^2, 63 mJ/cm^2 for gold nanorods and gold shells respectively (Fig. 8). The bubbles created local images with the diameter about 1 μm and specific and strong symmetrical PT-responses due to optical scattering of the probe laser beam that decreases axial intensity of probe laser beam. PT-responses (Fig. 7b, c) show the bubble expansion to the maximal diameter and the follow up collapse with the total lifetime being 50 ns for the gold rods, 20 ns for gold spheres, and 200 ns for the gold shells.

The most important result that we have discovered for these samples was that the level of PT signal immediately after the collapse of the bubble has indicated the initial level that corresponds to the temperature of the irradiated volume being equal to that before laser pulse (Fig. 8b, c). This result was observed for all types of studied NPs with the only difference being the lifetime of the bubble (Fig. 7). This means that the temperature of the irradiated volume outside the bubbles did not did not change during and after the bubble generation. The absence of any increase of the media temperature can also be seen at PT image: irradiated area between the bubbles and within the aperture of pump laser pulse did not differ from non-irradiated area outside pump beam aperture (Fig. 8). Therefore during the generation of laser induced bubbles around "active" NPs the temperature outside bubbles almost did not alter from the initial temperature. Also we did not observe any signs of the oscillation of the bubble, which implies that bubble dynamics is not truly adiabatic.

This result also can be interpreted as "thermal insulation" of the surrounding liquid from NP-mediated photothermal impact. In this case the volume having a high temperature is comparable to the

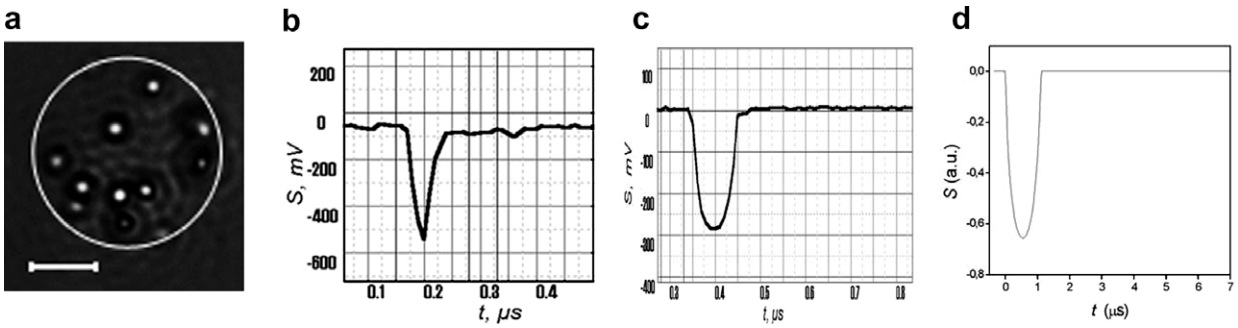

Fig. 8. Time-resolved image (a) and time-response (b) of laser-induced bubbles around gold rods 14 × 45 nm (pump pulse: 532 nm, 11 J/cm^2) and (c) time-response of laser-induced bubbles around gold shells 170/8 nm (pump pulse: 532 nm, 63 mJ/cm^2), (d) photothermal response of laser-induced adiabatic bubble calculated for adiabatic conditions. Y-axis is for the output of the photodetector (mV). Image scale bar is 4 μm.

volume of NPs plus the volume occupied by the bubble at its early stage of expansion (the temperature inside the bubble when it reaches for its maximal radius can be even lower than the ambient temperature because the temperature inside the bubble decreases during its expansion). Despite a significant increase of laser fluence from 1 to 10 J/cm^2 the bulk laser-induced temperature of the irradiated media has decreased due to localization of released thermal energy inside the bubbles. Thus the bubble mode may provide thermal confinement of irradiated media that can be characterized by temporal confinement factor of 15 for the shells (3 μs–200 ns), 60 for the rods (3 μs–50 ns), 150 for the spheres (3 μs–20 ns) and spatial confinement factor of more than 1000.

4. Conclusions

1. Nanoparticles may improve vaporization and boiling. Providing specific task and conditions the nanoparticles may be used in passive or active modes.
2. Passive mode assumes that NPs do not generate thermal energy, which is homogeneously produced by the fluid. Under these conditions application of the nanoparticles may decrease boiling energy threshold by half relatively to that in pure fluid.
3. Active mode assumes that NPs act as converters of optical energy into thermal one. This mode allows to decrease boiling energy threshold by 10–100 times relatively to that in pure fluid.
4. In the both modes actual thresholds depend upon the size and concentration of the nanoparticles.
5. Additionally we have demonstrated that the applications of photothermal microscopy allows to visualize individual bubbles generation in transparent mini-evaporator.

References

[1] J. Mitrovic, How to create an efficient surface for nuclear boiling?, Int J. Therm. Sci. 45 (2006) 1–15.
[2] L. Vasiliev, A. Zhuravlyov, A. Shapovalov, V. Litvinenko, Vaporization heat transfer in porous wicks of evaporators, Arch. Thermodyn. 25 (3) (2004) 47–59.
[3] L. Vasiliev, D. Lapotko, E. Lukianova, A. Zhurablyov, A. Shapovalov, L. Vasiliev Jr., Two phase heat transfer enhancement in micro channels and heat pipe evaporators with nano porous structures, in: Proceedings of the 14th International Heat Pipes Conference (14th IHPC), Florianopolis, Brazil, April 22–27, 2007.
[4] L. Vasiliev, A. Zhuravlyov, A. Shapovalov, L. Vasiliev Jr., Microscale two phase heat transfer enhancement in porous structures, in: Proceedings of the 13th International Heat Transfer Conference, Sydney, Australia, 3–18 August, 2006.
[5] X. Xie, H. Lee, W. Youn, M. Choi, Nano-fluids containing multiwalled carbon nano-tubes and their enhanced therma conductivities, J. Appl. Phys. 94 (8) (2003) 4967–4971.
[6] H.E. Patel, S.K. Das, T. Sundararajan, A.S. Nair, B. George, T. Pradeep, Thermal conductivities of naked and monolayer protected metal nano-particles based nano-fluids: manifestation of anomalous enhancement and chemical effects, Appl. Phys. Lett. 83 (14) (2003) 2931–2933.
[7] T. Cho, I. Baek, J. Lee, S. Park, Preparation of nano-fluids containing suspended silver particles for enhancing fluid thermal conductivity of fluids, J. Ind. Eng. Chem. 11 (3) (2005) 400–406.
[8] Y. Xuan, Q. Li, Heat transfer enhancement of nano-fluids, Int. J. Heat Fluid Flow 21 (2000) 58–64.
[9] S.U.S. Choi, J.A. Eastman, S. Li, W. Yu, J. Thompson, Anomalously increased effective thermal conductivities of ethylene glycol-based containing copper nano-particles, Appl. Phys. Lett. 78 (6) (2001) 718–720.
[10] Y. Xuan, Q. Li, Investigation on convective heat transfer and flow features of nano-fluids, J. Heat Transfer 125 (2003) 151–155.
[11] S.K. Das, N. Putra, P. Thiesen, W. Roetzel, Temperature dependence of thermal conductivity enhancement for nano-fluids, J. Heat Transfer 125 (2003) 567–574.
[12] X.Q. Wang, A.S. Mujumdar, Heat transfer characteristics of nanofluids: a review, Int. J. Therm. Sci. 46 (2007) 1–19.
[13] W. Daungthongsuk, S. Wongwises, A critical review of convective heat transfer of nanofluid, Renew. Sust. Energ. Rev. 11 (2007) 797–817.
[14] V. Trisaksria, S. Wongwises, Critical review of heat transfer characteristics of nanofluids, Renew. Sust. Energ. Rev. 11 (2007) 512–523.
[15] C.H. Li, G.P. Peterson, The effect of particle size on the effective thermal conductivity of Al_2O_3-water nanofluids, J. Appl. Phys. 101 (2007) 044312.
[16] D. Lapotko, E. Lukianova, Laser-induced micro-bubbles in cells, Int. J. Heat Mass Transfer 48 (1) (2005) 227–234.
[17] D. Lapotko, E. Lukianova, A. Iraevsky, A Selective laser nano-thermolysis of human leukemia cells with microbubbles generated around clusters of gold nanoparticles, Lasers Surg. Med. 38 (1) (2006) 631–642.
[18] V. Letokhov, Effects of transient local heating of spatially and spectrally heterogeneous biotissue by short laser pulses, Nuovo Cimento D 13 (1991) 939–948.
[19] S.L. Ceccio, C.E. Brennen, Observations of the dynamics and acoustics of travelling bubble cavitation, J. Fluid Mech. 233 (1991) 633–660.
[20] M.S. Plesset, A. Prosperetti, Bubble dynamics and cavitation, Ann. Rev. Fluid Mech. 9 (1977) 145–185.
[21] J.E. Shepherd, B. Sturtevant, Rapid evaporation near the superheat limit, J. Fluid Mech. 121 (1982) 379–402.
[22] B.S. Gersman, Theoretical modeling of laser induced explosive pressure generation and vaporization in pigmented cells, Proc. SPIE 3902 (2000) 41–52.
[23] D. Lapotko, G. Kuchinsky, Optothermal microscope, in: F. Scudiery, M. Bertolotti (Eds.), Photoacoustica and Optothermal Phenomena, AIP, Rome, 1998, pp. 184–186.
[24] D. Lapotko, E. Lukianova, A. Shnip, Photothermal responses of individual cells, J. Biomed. Opt. 10 (1) (2004) 014006.
[25] H. Liao, J. Hafner, Gold nanorod bioconjugate, Chem. Mater. 17 (2005) 4636–4641.
[26] C. Loo, A. Lowery, N. Halas, J. West, R. Drezek, Immunotargeted nanoshells for integrated cancer imaging and therapy, Nano Lett. 5 (2005) 709–711.